

# *In-situ* UV-Raman study on soot combustion over TiO<sub>2</sub> or ZrO<sub>2</sub>-supported vanadium oxide catalysts

LIU Jian<sup>1</sup>, ZHAO Zhen<sup>1†</sup>, XU ChunMing<sup>1</sup>, DUAN AiJun<sup>1</sup>, JIANG GuiYuan<sup>1</sup>, GAO JinSen<sup>1†</sup>, LIN WenYong<sup>2</sup> & WACHS Israel E.<sup>2</sup>

<sup>1</sup> State Key Laboratory of Heavy Oil Processing, China University of Petroleum, Beijing 102249, China;

<sup>2</sup> *In-situ* Molecular Characterization and Catalysis Laboratory, Department of Chemical Engineering, Lehigh University, Bethlehem, PA 18015, USA

UV-Raman spectroscopy was used to study the molecular structures of TiO<sub>2</sub> or ZrO<sub>2</sub>-supported vanadium oxide catalysts. The real time reaction status of soot combustion over these catalysts was detected by *in-situ* UV-Raman spectroscopy. The results indicate that TiO<sub>2</sub> undergoes a crystalline phase transformation from anatase to rutile phase with the increasing of reaction temperature. However, no obvious phase transformation process is observed for ZrO<sub>2</sub> support. The structures of supported vanadium oxides also depend on the V loading. The vanadium oxide species supported on TiO<sub>2</sub> or ZrO<sub>2</sub> attain monolayer saturation when V loading is equal to 4 (4 is the number of V atoms per 100 support metal ions). Interestingly, this loading ratio (V<sub>4</sub>/TiO<sub>2</sub> and V<sub>4</sub>/ZrO<sub>2</sub>) gave the best catalytic activities for soot combustion reaction on both supports (TiO<sub>2</sub> and ZrO<sub>2</sub>). The formation of surface oxygen complexes (SOC) is verified by *in-situ* UV Raman spectroscopy and the SOC mainly exist as carboxyl groups during soot combustion. The presence of NO in the reaction gas stream can promote the production of SOC.

vanadium oxide, catalyst, UV-Raman, *in-situ*, soot combustion

## 1 Introduction

Supported vanadium oxide catalysts have been widely applied in many catalytic reactions such as the selective oxidation of hydrocarbon, the selective catalytic reduction (SCR) of nitrogen oxides with ammonia and the oxidative dehydrogenation of alkanes. The catalytic properties of these catalysts depend on the structures of the supported vanadia species, support material and VO<sub>x</sub> concentration. The complete understanding of their catalytic properties requires the determination of the structure-activity relationship of these catalytic materials. However, the exact structures of the amorphous vanadia and their bonding to the support are still in controversy and have, therefore, become the focus of several recent studies<sup>[1-4]</sup>. The structures of the supported vanadium oxides have been investigated by many techniques. The spectroscopic study of the surface metal oxide species

will lead to the deeper insights into the nature of the surface active sites and active phases which are responsible for the catalytic performances. Raman spectroscopy is one of the proper techniques used for the characterization of the supported oxide catalysts since the Raman signals can give the direct information on the surface coordination structures of the supported metal oxide species<sup>[5,6]</sup>. However, its application for supported oxides has been limited by the strong fluorescence interference in conventional visible Raman spectroscopy. Li et al. have successfully applied UV Raman spectroscopy for the study of supported oxide catalysts. UV Raman spectroscopy can successfully avoid the surface

Received April 9, 2007; accepted October 17, 2007

doi: 10.1007/s11426-008-0027-2

<sup>†</sup>Corresponding author (email: zhenzhao@cup.edu.cn; jsgao@cup.edu.cn)

Supported by the National Natural Science Foundation of China (Grant Nos. 20473053, 20773163 and 20525621), the Beijing Natural Science Foundation (Grant No. 2062020), and the 863 Program of China (Grant No. 2006AA06Z346)

fluorescence which often obscures the normal Raman spectra<sup>[6–10]</sup>.

Recently, vanadium-based catalysts are considered one of the most promising systems for the combustion of diesel soot<sup>[11–14]</sup>. Soot is a carbonaceous material made of amorphous carbon particles containing a variable amount of toxic hydrocarbons and is the main environmental pollutant present in the exhaust gas emitted from diesel engines. Collection of soot in a monolithic filter and simultaneous oxidation is considered to be a good option to minimize its environmental contamination. However, the solid soot can only be burnt off during a short period of time at temperatures above 600°C. Such high temperatures cannot be achieved in the exhaust stream under typical engine operating conditions. To overcome this problem, oxidation catalysts are needed to increase the oxidation rate of carbon at lower temperatures. A great deal of attention has been paid in the last twenty years to the research of soot catalytic combustion. Some catalytic systems such as vanadium-based catalysts<sup>[11–14]</sup>, cerium-based catalysts<sup>[15–17]</sup>, noble metal containing Pt catalysts<sup>[18,19]</sup>, perovskite or spinel complex oxide catalysts<sup>[20–24]</sup> have acquired apparent progress for soot catalytic combustion. Several problems still remain unsolved, although the amount of the work towards a better understanding is impressive. In particular, the reaction mechanism of the catalytic combustion of soot remains unclear. The deep black color of soot makes it very difficult to acquire some useful information about the catalytic oxidation of soot under real reaction conditions. The combination of fundamental molecular structural information and *in-situ* techniques has resulted in a powerful tool for catalysis science, which allows for the development of a molecular-level understanding of structure-activity/selectivity relationships for catalytic reactions. In this work, the *in-situ* UV Raman technique was firstly employed to investigate the mechanism of soot combustion over supported vanadia catalysts. It was verified that the formation of surface oxygen complexes (SOC), which mainly exist as carboxyl groups, was the main reaction process during the soot combustion.

## 2 Experimental section

### 2.1 Catalyst preparation

All of the chemicals used for catalyst preparation were

of analytical grade. The supports used in this study were TiO<sub>2</sub> (anatase, 60–100 mesh, 9 m<sup>2</sup>/g) and ZrO<sub>2</sub> (60–100 mesh, 2 m<sup>2</sup>/g). Vanadium was introduced onto the supports by an incipient-wetness impregnation method with a variable NH<sub>4</sub>VO<sub>3</sub> content between 0 and 20%. The two types of supported vanadia catalysts are denoted as V<sub>*m*</sub>/TiO<sub>2</sub> or V<sub>*m*</sub>/ZrO<sub>2</sub>, respectively, where *m* is the number of V atoms per 100 support metal ions (*m* = 0, 0.1, 1, 4, 10, 20). During the impregnation, the citric acid (equi-molar ratio to metal vanadium) was added to the solution for promoting the dissolution of NH<sub>4</sub>VO<sub>3</sub>. After impregnation, the catalyst precursors were dried at 120°C for 12 h and then calcined at 700°C for 4 h in static air.

### 2.2 Catalyst characterization

**2.2.1 Ambient UV-Raman measurement.** UV-Raman spectra of supported vanadium oxides were collected at room temperature with a Jobin Yvon LabRam-HR spectrometer equipped with a confocal microscope, 2400/900 grooves/mm gratings and a notch filter. The notch filter allows for the use of a one-stage monochromator in this system that significantly enhances the intensity of the detected photons. The laser excitation at 325 nm was generated from a He-Cd laser (Kimmon, Model: IK5751I-G, 30 mW). The scattered photons were directed and focused onto a single stage monochromator and measured with a UV sensitive LN<sub>2</sub>-cooled CCD detector (Yvon LabRam CCD-3000 V). The notch filter for the UV spectra had a ~300 cm<sup>-1</sup> cut off. The samples were in powder form and only 5–10 mg was usually loosely spread onto a glass slide below the confocal microscope. The spectrometer resolution was less than 2 cm<sup>-1</sup>.

**2.2.2 *In-situ* UV-Raman measurement.** For the *in-situ* Raman studies of supported vanadia catalysts were loaded in powder form into an *in-situ* cell (Linkam, TS1500) that allowed for reaction and sample treatments such as dehydration. The quartz cell is capable of operating up to 650°C. The *in-situ* Raman spectra were collected at each reaction temperature under specific gaseous conditions by flowing 10% O<sub>2</sub>/He (50 mL/min) or (0.2% NO + 5% O<sub>2</sub>)/He (50 mL/min).

### 2.3 Catalytic activity measurement

The catalytic activities of the prepared catalysts for soot oxidation were evaluated with temperature-programmed oxidation reactions (TPO) and carried out in a fixed-bed

tubular quartz system<sup>[13]</sup>. The reaction temperature was controlled through a PID-regulation system consisted of the measurements of a K-type thermocouple and varied from 200°C to 600°C at a rising rate of 2°C/min during each TPO run. Printex-U, which was supplied by Degussa, was used as model soot. Its primary particle size was 25 nm and specific surface area was 100 m<sup>2</sup>/g. The catalyst and soot (10:1 w/w) were carefully mixed in an agate mortar to ensure a thorough mixing<sup>[13,25]</sup>, and 100 mg of the mixture was placed in the tubular quartz reactor ( $\phi = 8$  mm). Reactant gases containing 5% O<sub>2</sub> and 0.2% NO balanced with He were passed through a mixture of the catalyst and soot at a flow rate of 200 mL/min. The outlet gas composition from the reactor passed through a 1 cm<sup>3</sup> sampling loop of a six-point gas-sampling valve before it was being injected into an on-line gas chromatograph (GC). The GC with a flame ionization detector (FID) was used to analyze the concentrations of CO and CO<sub>2</sub>. In the analysis, a Porapak N column was used for separation and was followed by converting carbon containing species into methane over a Ni catalyst at 380°C for detection.

### 3 Results

#### 3.1 UV-Raman spectroscopic characterization of V<sub>m</sub>/TiO<sub>2</sub> and V<sub>m</sub>/ZrO<sub>2</sub> catalysts

Figure 1 shows the Raman spectra of hydrated V<sub>m</sub>/TiO<sub>2</sub> samples. The bands at 399, 514, and 638 cm<sup>-1</sup> are due to the Raman-active modes of anatase phase with the symmetries of B<sub>1g</sub>, A<sub>1g</sub>, and E<sub>g</sub>, respectively<sup>[26,27]</sup>. The peak at 323 cm<sup>-1</sup> is assigned to the  $\delta$  vibration of V—O—V<sup>[28]</sup>. At medium V loading, the peaks at 781, 804 and 956 cm<sup>-1</sup> are observed for V<sub>1</sub>/TiO<sub>2</sub>, V<sub>4</sub>/TiO<sub>2</sub>, V<sub>10</sub>/TiO<sub>2</sub> and V<sub>20</sub>/TiO<sub>2</sub> samples. The former two bands are attributable to the stretching vibration of V—O—V, and the last one is assigned to the terminal V=O stretching vibrations of the polyvanadates. At high V loading (V<sub>10</sub>/TiO<sub>2</sub> and V<sub>20</sub>/TiO<sub>2</sub> samples), a strong vibration band, located at 994 cm<sup>-1</sup>, is primarily due to the symmetric stretch of V=O groups in the bulk V<sub>2</sub>O<sub>5</sub>.

In the Raman spectra of V<sub>m</sub>/TiO<sub>2</sub> samples, the intensity of the anatase peaks remains virtually unchanged when  $m$  is less than 4, indicating that V coverage does not reach monolayer saturation. But when vanadium loading exceeds 4, the increment in V content markedly reduces the intensity of the anatase absorption peaks

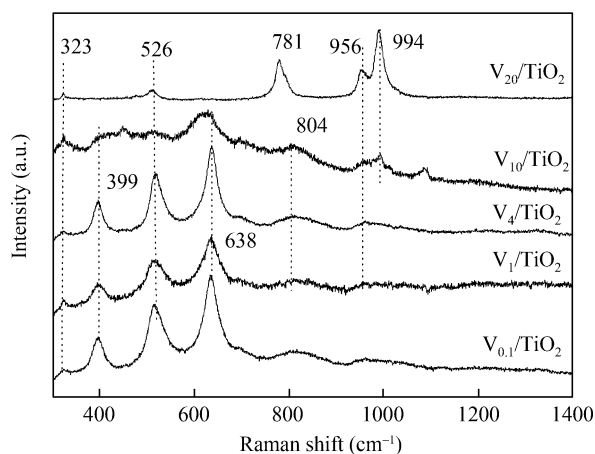


**Figure 1** The UV-Raman spectra of V<sub>m</sub>/TiO<sub>2</sub> catalysts ( $m = 0.1, 1, 4, 10, 20$ ).

Thus when  $m$  is higher than 4 exceeding the requirement of monolayer coverage, V<sub>2</sub>O<sub>5</sub> phase is formed, present in micro-crystallites. V<sub>2</sub>O<sub>5</sub> micro-crystallites shield the Raman absorption by TiO<sub>2</sub> surface. Therefore, V<sub>m</sub>/TiO<sub>2</sub> samples achieve the monolayer saturation dispersion when  $m$  is equal to 4 according to the above UV-Raman results.

Figure 2(a) shows the Raman spectra of hydrated V<sub>m</sub>/ZrO<sub>2</sub> samples ranging from 300 to 1400 cm<sup>-1</sup>. The bands at 334, 377, 472, 558, and 634 cm<sup>-1</sup> are assigned to the Raman-active modes B<sub>g</sub>, B<sub>g</sub>, A<sub>g</sub>, A<sub>g</sub>, and A<sub>g</sub> for monoclinic phase of ZrO<sub>2</sub>. The weak peak at 312 cm<sup>-1</sup> indicates that a small amount of ZrO<sub>2</sub> with tetragonal phase is present in the sample. Some small bands between 472 and 634 cm<sup>-1</sup>, attributable to the monoclinic phase of ZrO<sub>2</sub>, are also observed<sup>[29-31]</sup>. Similar to the results of the Raman spectra of V<sub>m</sub>/TiO<sub>2</sub> samples, the intensity of the tetragonal or monoclinic ZrO<sub>2</sub> Raman peaks is almost unchanged when  $m$  is less than 4. However, when vanadium loading exceeds 4, the increment in V content causes significant decrease in the intensity of the ZrO<sub>2</sub> absorption bands. This result also indicates that V<sub>m</sub>/ZrO<sub>2</sub> samples attain the monolayer coverage on ZrO<sub>2</sub> surface. To find out the structures of vanadium oxide on ZrO<sub>2</sub> support, the Raman spectra of V<sub>m</sub>/ZrO<sub>2</sub> samples ranging from 700 to 1400 cm<sup>-1</sup> were measured as shown in Figure 2(b). At low V loading, a shoulder peak from 995 to 1030 cm<sup>-1</sup> appears suggesting the presence of monovanadate species along with ZrV<sub>2</sub>O<sub>7</sub>. With the increase of vanadium loading, the sample shows a broad band from 800 to 980 cm<sup>-1</sup>, indicative of polyvanadate species. Further increase in V loading

causes a decrease in intensity of the broad band. Meanwhile, two peaks appear at 778 and 988  $\text{cm}^{-1}$ , which are attributed to  $\text{ZrV}_2\text{O}_7$ <sup>[30]</sup>. These results are in agreement with that by Olthof et al., who reported  $\text{ZrV}_2\text{O}_7$  formation accompanied by the  $\text{ZrO}_2$  phase from tetragonal to monoclinic phase. The results here suggest that  $\text{ZrV}_2\text{O}_7$  is formed by the reaction of polyvanadate surface species interacting with  $\text{ZrO}_2$  as it starts to form a monoclinic phase of  $\text{ZrO}_2$ <sup>[29]</sup>.

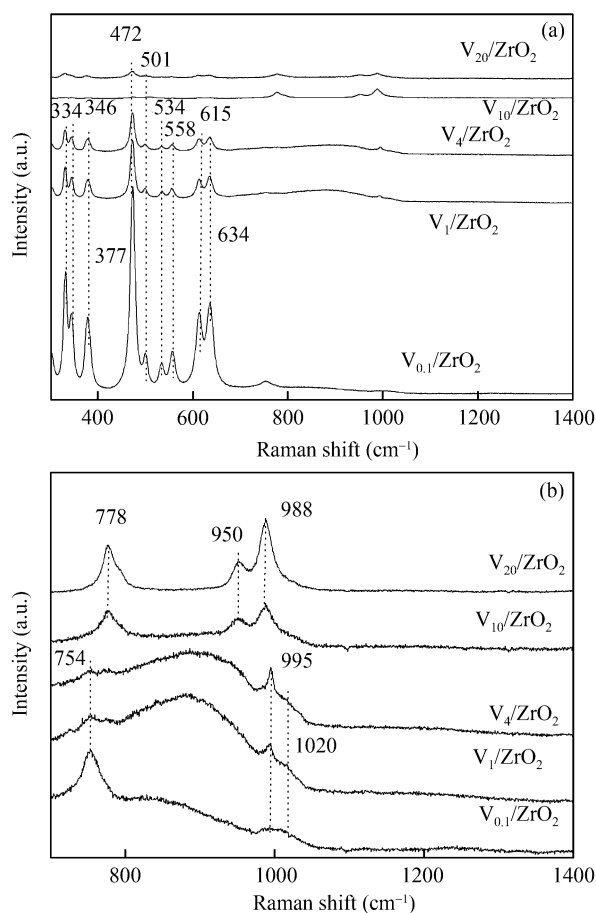


**Figure 2** The UV-Raman spectra of  $\text{V}_m/\text{ZrO}_2$  catalysts ( $m = 0.1, 1, 4, 10, 20$ ). (a) 300–1400  $\text{cm}^{-1}$ ; (b) 700–1400  $\text{cm}^{-1}$ .

### 3.2 Catalytic activity

The catalytic activity tests were performed according to the reported method<sup>[13]</sup>. The main product is  $\text{CO}_2$  for soot combustion over  $\text{V}_m/\text{TiO}_2$  or  $\text{V}_m/\text{ZrO}_2$  catalysts. The peak temperature ( $T_p$ ) at which the rate of  $\text{CO}_2$  formation peaked was used as a parameter to evaluate the catalytic performances of the catalysts for soot combustion. Figure 3(a) shows  $\text{CO}_2$  concentration/temperature plots for soot combustion over  $\text{V}_m/\text{TiO}_2$  catalysts. From Figure 3(a), it can be seen that for the titania-based catalysts,

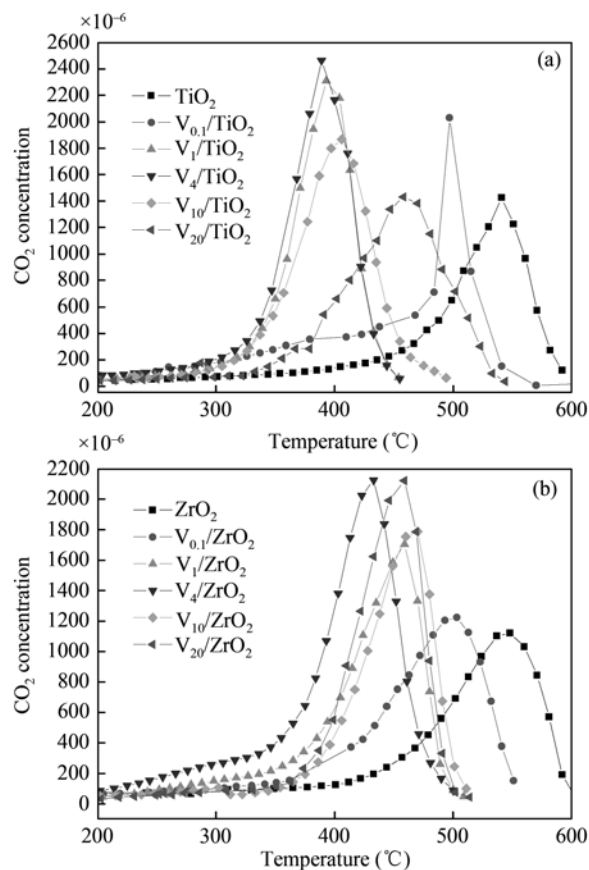


**Figure 3** The  $\text{CO}_2$  concentration for the catalytic combustion of soot over the  $\text{V}_m/\text{TiO}_2$  and  $\text{V}_m/\text{ZrO}_2$  catalysts ( $m = 0, 0.1, 1, 4, 10, 20$ ). (a)  $\text{V}_m/\text{TiO}_2$ , (b)  $\text{V}_m/\text{ZrO}_2$ .

$T_p$  decreases as vanadium loading increases for low V content samples ( $m \leq 4$ ), while at high V loading ( $m > 4$ )  $T_p$  increases with the increase of vanadium loading. This suggests that the highest activity is reached when a monolayer of vanadium oxide covers on the surface. As shown in Figure 3(b), similar results were also obtained for soot combustion over  $\text{V}_m/\text{ZrO}_2$  catalysts. The difference in the peak intensity of  $\text{CO}_2$  concentration is due to the different selectivity of  $\text{CO}_2$  for soot combustion over  $\text{V}_m/\text{TiO}_2$  or  $\text{V}_m/\text{ZrO}_2$  catalysts.

### 3.3 UV-Raman spectrum of soot

Figure 4 shows the typical UV-Raman spectrum of Printex-U. A strong sharp peak appears at 1585  $\text{cm}^{-1}$  and a shoulder peak at 1365  $\text{cm}^{-1}$ . According to the literature<sup>[32–34]</sup>, the spectrum of soot generally exhibit two broad and strong overlapping peaks with intensity maxima at  $\sim 1580 \text{ cm}^{-1}$  and at  $\sim 1350 \text{ cm}^{-1}$ . The band at around 1580  $\text{cm}^{-1}$  is corresponding to an ideal graphitic lattice vibration mode with  $E_{2g}$  symmetry, and the band at  $\sim 1360 \text{ cm}^{-1}$  is assigned to a disorder graphitic lattice

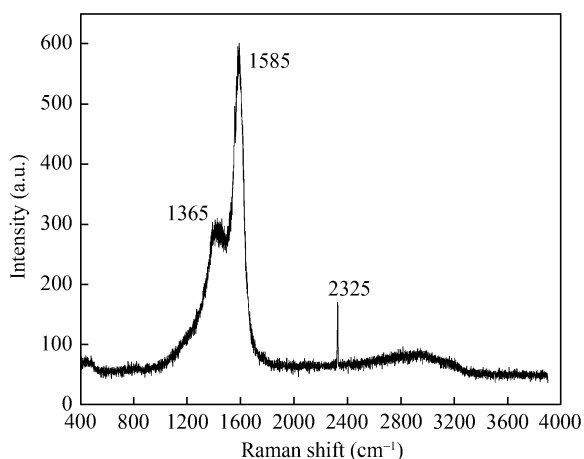


Figure 4 The UV-Raman spectrum of Printex-U.

vibration mode with  $A_{1g}$  symmetry<sup>[32–34]</sup>.

### 3.4 *In-situ* UV-Raman spectra

In order to investigate the reaction mechanism of soot combustion over  $V_m/TiO_2$  or  $V_m/ZrO_2$  catalysts,  $V_4/TiO_2$  or  $V_4/ZrO_2$  catalysts, the most active ones among all different loading ratios were used for *in-situ* Raman study.

Figure 5 shows the *in-situ* UV-Raman spectra of  $V_4/TiO_2$  catalyst for soot combustion in  $(NO+O_2)/He$  atmosphere as a function of temperature. The peaks below  $1200\text{ cm}^{-1}$  are due to the vibration of vanadyl species or anatase. The peak at  $1585\text{ cm}^{-1}$  corresponds to an ideal graphitic lattice vibration mode with  $E_{2g}$  symmetry. Several new peaks at 1545, 1618 and  $1675\text{ cm}^{-1}$  shows up in the Raman spectra. The former two peaks may be attributed to the formation of SOC on Printex-U in the presence of  $V_4/TiO_2$  catalyst<sup>[35]</sup>, and the last one may be due to the  $\nu_{as}$  vibration of  $NO_2$ <sup>[36,37]</sup>. According to the literature, the band at  $1545\text{ cm}^{-1}$  is ascribed to the ring stretching vibrations of aromatic moieties, and the band at  $1618\text{ cm}^{-1}$  may be assigned to the  $\nu_A$  vibration of  $COO^-$  and benzene ring stretching. It indicates that the SOC mainly exist as carboxyl groups<sup>[35]</sup>. With the increase of the reaction temperature, the intensity of the peak at  $1675\text{ cm}^{-1}$  gradually decreases, and when the reaction temperature increases to  $300^\circ\text{C}$ , the peak disappears. This phenomenon indicates that  $NO_2$  has decomposed due to the thermodynamic instability of  $NO_2$  at high temperature. However, a small amount of  $NO_2$  was produced again at  $650^\circ\text{C}$  during the reaction. A reasonable explanation is that the complete oxidation of soot disturbs the chemical equilibrium of NO and  $NO_2$ . As a result, a very weak peak at  $1675\text{ cm}^{-1}$  reappears at

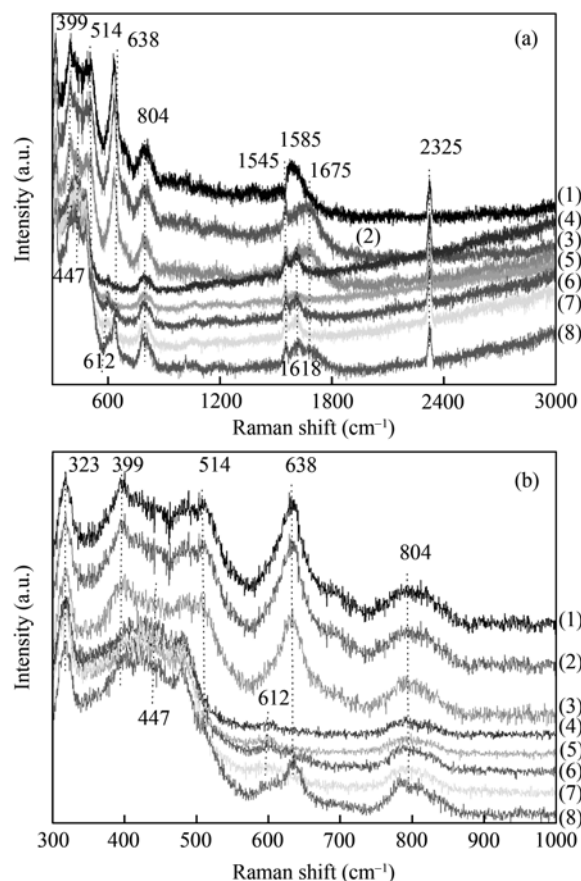


Figure 5 The *in situ* UV-Raman spectra of  $V_4/TiO_2$  catalysts during soot combustion in  $(NO+O_2)/He$  atmosphere as a function of temperature. Reaction temperature: (1) room temperature, (2)  $100^\circ\text{C}$ , (3)  $200^\circ\text{C}$ , (4)  $300^\circ\text{C}$ , (5)  $400^\circ\text{C}$ , (6)  $500^\circ\text{C}$ , (7)  $600^\circ\text{C}$ , (8)  $650^\circ\text{C}$ . (a)  $300\text{--}3000\text{ cm}^{-1}$ ; (b)  $300\text{--}1000\text{ cm}^{-1}$ .

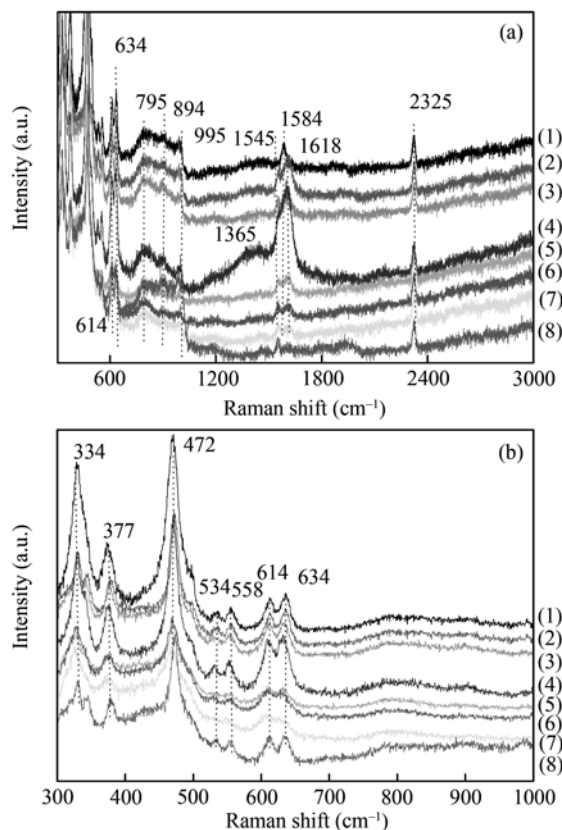
high temperature. For  $V_4/TiO_2$  catalyst, as shown in Figure 3(a), the reaction of soot combustion has completed when the reaction temperature reaches to  $450^\circ\text{C}$ . A contradiction to the explanation is that the  $NO_2$  vibration peak did not reappear at  $500^\circ\text{C}$ , but shows up at  $650^\circ\text{C}$  instead. This mismatch may be caused by the difference in the way catalytic activity measurements and *in-situ* UV-Raman investigation for soot combustion was carried out. In the catalytic activity measurements, the rising rate of temperature was  $2^\circ\text{C}/\text{min}$  during each TPO run. Because of the low temperature ramping rate, by the time temperature reaches  $450^\circ\text{C}$ , soot combustion has completed. Due to technical difficulties, it is not practical to collect Raman spectrum during each TPO run. Each UV-Raman spectrum was collected at a certain reaction temperatures and the temperature was quickly went up to the desired targets at a ramping rate of  $10^\circ\text{C}/\text{min}$ . As a consequence of the high temperature

ramping rate, soot combustion finishes late until the reaction temperature reached 600°C. Therefore, the reaction came through short time raising temperature 100°C and soot combustion continued until the reaction temperature reached 600°C. Thus, as shown in Figure 5, the NO<sub>2</sub> vibration peak did not show up at 500°C and 600°C, and until temperature reaches 650°C.

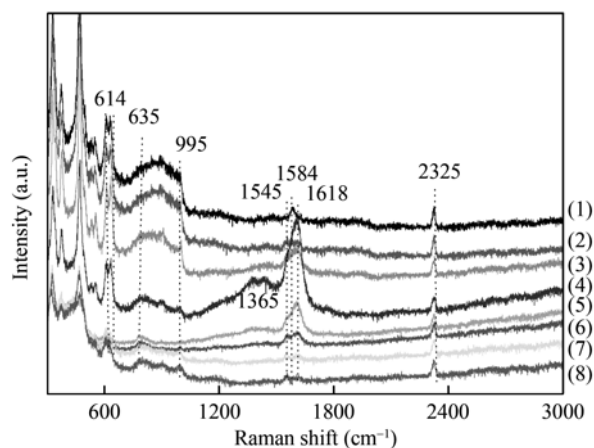
In the process of soot combustion over V<sub>4</sub>/TiO<sub>2</sub> catalyst with the increasing of reaction temperature the anatase-rutile phase transformation of TiO<sub>2</sub> was observed as evidenced in the *in-situ* Raman spectroscopic measurements. Shown in Figure 5(b) are the spectra acquired at different temperatures. Below 300°C, the bands at 399, 514, and 638 cm<sup>-1</sup>, characteristic of the symmetric vibration of anatase phase<sup>[27]</sup>, are displayed. However, above 300°C, the typical Raman bands attributing to rutile phase appear at 447 and 612 cm<sup>-1</sup>. These two bands can be ascribed to the E<sub>g</sub> and A<sub>1g</sub> modes of rutile phase, respectively.

Figure 6 shows the *in-situ* UV-Raman spectra of V<sub>4</sub>/ZrO<sub>2</sub> catalyst for soot combustion in (NO+O<sub>2</sub>)/He atmosphere at different temperatures. The peaks below 1200 cm<sup>-1</sup> are due to the vanadyl or zirconium oxides. The peak at 1584 cm<sup>-1</sup> is corresponding to an ideal graphitic lattice vibration mode with E<sub>2g</sub> symmetry and that at 1365 cm<sup>-1</sup> is assigned to the A<sub>1g</sub> symmetry vibration of the disorder graphitic lattice. When reaction temperature exceeds 100°C, two new peaks at 1545 and 1618 cm<sup>-1</sup>, which may be attributed to the formation of carboxyl groups, appear during soot oxidation on V<sub>4</sub>/ZrO<sub>2</sub> catalyst<sup>[35]</sup>. With the increase of the reaction temperature, the intensities of the peaks gradually increase, indicating that the vibration enhances, i.e., the concentration of SOC increases. However, when reaction temperature exceeds 300°C, the intensities of the both peaks gradually decrease and disappear at last. The disappearance of the peaks at higher temperature may result from the depletion of SOC, and in essence from the depletion of soot as at higher temperature soot is shown to be consumed quickly. The argument is supported by the UV Raman spectra of V<sub>4</sub>/ZrO<sub>2</sub> catalyst in the range from 300 to 1000 cm<sup>-1</sup>, shown in Figure 6(b). Phase transformation process of ZrO<sub>2</sub> are not expected to take place within our experimental temperature range as the monoclinic ZrO<sub>2</sub> is very stable below 1170°C<sup>[31]</sup>.

Figure 7 shows the *in-situ* UV-Raman spectra of



**Figure 6** The *in situ* UV-Raman spectra of V<sub>4</sub>/ZrO<sub>2</sub> catalysts during soot combustion in (NO+O<sub>2</sub>)/He atmosphere as a function of temperature. Reaction temperature: (1) room temperature, (2) 100°C, (3) 200°C, (4) 300°C, (5) 400°C, (6) 500°C, (7) 600°C, (8) 650°C. (a) 300–3000 cm<sup>-1</sup>; (b) 300°C, 1000 cm<sup>-1</sup>.



**Figure 7** The *in situ* UV-Raman spectra of V<sub>4</sub>/ZrO<sub>2</sub> catalysts during soot combustion in O<sub>2</sub>/He atmosphere as a function of temperature. Reaction temperature: (1) room temperature, (2) 100°C, (3) 200°C, (4) 300°C, (5) 400°C, (6) 500°C, (7) 600°C, (8) 650°C.

V<sub>4</sub>/ZrO<sub>2</sub> catalyst for soot combustion in O<sub>2</sub>/He atmosphere as a function of temperature. The positions of the vibration peaks are basically unchanged compared with

the UV-Raman spectra in Figure 6(a). Therefore, the peaks at 1545 and 1618  $\text{cm}^{-1}$  do not originate from the stretching vibration of the species containing nitrogen. By cross comparison of Figure 6(a) with Figure 7, it can be found that the peak intensities at 1545 and 1618  $\text{cm}^{-1}$  are much lower in Figure 7 in the latter case than in the former case. This suggests that the formation of SOC is more favored in (NO+O<sub>2</sub>)/He atmosphere than in O<sub>2</sub>/He atmosphere.

## 4 Discussion

### 4.1 The *in-situ* UV Raman characterization of the phase transformation of supports and the structures of supported vanadium oxides

TiO<sub>2</sub> and ZrO<sub>2</sub> have been widely studied as the supports in catalysis because of their unique properties. For TiO<sub>2</sub>, the two major kinds of crystalline phases (i.e., anatase and rutile) exhibit different physical and chemical properties. It is well-known that the crystalline phase of TiO<sub>2</sub> plays a significant role in catalytic reactions, and the anatase phase is more suitable for catalysts and supports. For ZrO<sub>2</sub>, there exist three different crystalline phases including monoclinic, which is stable below 1170°C; tetragonal, which is stable between 1170°C and 2370°C; and cubic, stable from 2370°C to its melting temperature at 2680°C. In addition to monoclinic ZrO<sub>2</sub>, metastable tetragonal ZrO<sub>2</sub> can exist at room temperature. Ultraviolet Raman spectroscopy is a powerful tool for the study of catalyst support, such as TiO<sub>2</sub> and ZrO<sub>2</sub>. Some excellent studies have been done to understand the crystalline phase and phase transformation process of TiO<sub>2</sub> and ZrO<sub>2</sub> with UV-Raman techniques<sup>[27,31]</sup>. We expand the application for the determination of their structures and the catalytic properties of TiO<sub>2</sub>- or ZrO<sub>2</sub>-supported vanadia catalysts under the *in-situ* reaction conditions.

As shown in Figure 5(b), the peaks at 399, 514, and 638  $\text{cm}^{-1}$  disappear and several new peaks at 447 and 612  $\text{cm}^{-1}$  appear in the UV Raman spectroscopy of V<sub>4</sub>/TiO<sub>2</sub> sample at 300°C. This indicates that the crystalline phase transformation of TiO<sub>2</sub> from anatase phase to rutile phase occur at around 300°C. It has been reported that the phase transformation of TiO<sub>2</sub> from anatase to rutile takes place at 550°C and would be completed until up to 750°C<sup>[27]</sup>. The difference in the phase transformation temperatures from the reported one may be

caused by the presence of vanadia. The phase transformation temperature of TiO<sub>2</sub> was influenced by many factors such as the crystalline sizes and the presence of impurities. As prior to its utility, the catalysts had been calcined at 700°C and their crystalline sizes should have been fully grown. Thus, it appears that the small size effect is not the reason for the low phase transformation temperature of TiO<sub>2</sub>. The formation of a mixed oxide of vanadia with rutile TiO<sub>2</sub> has been reported. The low phase transformation temperature may be induced by the migration of vanadia into the TiO<sub>2</sub> lattice<sup>[29]</sup>. The spectra presented in Figure 5 show some evidences of rutile formation. The migration of vanadia into TiO<sub>2</sub> may explain the reduction in the temperature of phase transformation of TiO<sub>2</sub>. On the other hand, the migration can also partially illustrate the decrease in intensity of the stretching vibration of V—O—V at 804  $\text{cm}^{-1}$ .

For ZrO<sub>2</sub> support, as shown in Figure 6(b), no obvious phase transformation process was found. However, a little change can also be observed during the reaction. There are two main differences in the Raman spectra between the monoclinic phase and the tetragonal phase of zirconia, i.e., the intensity of the band at 472  $\text{cm}^{-1}$  is stronger than that of the band at 634  $\text{cm}^{-1}$  for the monoclinic phase. But the order is reversed for the tetragonal phase, and there are some small bands between 472 and 634  $\text{cm}^{-1}$  for the monoclinic phase, while these weak bands are absent for the tetragonal phase. Below 400°C, the intensity of peak at 634  $\text{cm}^{-1}$  is much stronger than that at 472  $\text{cm}^{-1}$ , and small vibration peaks at 534, 558, and 614  $\text{cm}^{-1}$  are also clear. These results indicate that the monoclinic phase is dominant in the sample. However, when reaction temperature reaches 400°C, the intensity of peak at 472  $\text{cm}^{-1}$  rapidly decreases, and small peaks between 472 and 634  $\text{cm}^{-1}$  become very weak. These results indicate that some tetragonal phase of ZrO<sub>2</sub> is also present in the sample.

Supported vanadium oxide has been a subject with considerable interest because it represents a kind of model catalysts for the analysis of the interactions among the oxide surfaces and support. It is generally accepted that at low V loadings isolated four-fold coordinated monovanadates species are present on the surface, characterized by a band at ~1030  $\text{cm}^{-1}$ , corresponding to a strong vibration of V=O bond. At higher V loadings, the broad V=O stretching bands appearing

in the lower frequency range (1000—900  $\text{cm}^{-1}$ ), are originated from the  $\text{V}=\text{O}$  stretch vibration of polymeric vanadyl species or  $\text{V}_x\text{O}_y$  “clusters” formed on the surface. And the bands below 900  $\text{cm}^{-1}$ , which can be assigned to  $\nu(\text{V}-\text{O}-\text{V})$ , also exist. The formation of crystalline bulk  $\text{V}_2\text{O}_5$  with a typical vibration band at 994  $\text{cm}^{-1}$  starts after the surface has been covered with a monolayer of different poly- and monovanadates species. These two-dimensional surface vanadium oxide species are believed to be the active redox sites, while crystalline bulk vanadium oxide is supposed to be less active than surface vanadyl species in catalytic reactions<sup>[13,35]</sup>. Consistent findings in the literature, when V loading is low ( $m = 0.1$  or 1), the vanadium oxide species supported on  $\text{TiO}_2$  or  $\text{ZrO}_2$  can be present as monomeric species and the peak is located at 1020  $\text{cm}^{-1}$ . With the increase of V loading, polymeric vanadium species emerge on the surface of the supports, and when V loading reaches 4, the V attains monolayer coverage on the support. Under this condition, the redox ability of the catalysts with monolayer saturation is the strongest. Given the tight contact between the catalyst and soot in our experiment, the influence of the contact condition for soot combustion may be neglected. Therefore,  $\text{V}_4/\text{TiO}_2$  and  $\text{V}_4/\text{ZrO}_2$  are the most active catalyst among all the  $\text{V}_m/\text{TiO}_2$  and  $\text{V}_m/\text{ZrO}_2$  samples.

#### 4.2 The mechanism of soot combustion over supported vanadium oxides

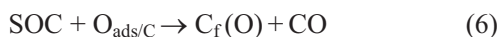
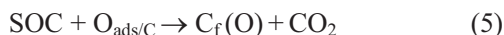
Elucidation of the mechanism of catalytic oxidation reactions of carbonaceous materials has been the subject of many researches over the last decades<sup>[38,39]</sup>. The formation and subsequent decomposition of SOC have been discussed in mechanistic studies of potassium- and calcium-catalyzed carbon oxidation. In the catalytic oxidation of graphite, chars and/or carbon black by metal oxides, a redox mechanism has been developed to explain experimental phenomena. In the mechanism, in the first step the catalyst is reduced by carbon first, followed by re-oxidation of the oxide by molecular oxygen. The formation of SOC on Printex-U in the presence of transition metal oxide catalysts has been reported by using IR technique. The three absorption bands could be identified in the spectra, located at 1257, 1607, and 1738  $\text{cm}^{-1}$ . The 1607  $\text{cm}^{-1}$  absorption peak is caused by aromatic stretching vibrations of the soot, which are enhanced by polar functional groups like quinine. The other two absorption bands have been assigned to oxy-

gen complexes formed on the soot surface: lactones (1738  $\text{cm}^{-1}$ ), and ether-like complexes (1257  $\text{cm}^{-1}$ ), respectively<sup>[40,41]</sup>. The intensity of the IR bands, i.e. the concentration of SOC, was found to increase with soot conversion. The 1257, 1607 and 1738  $\text{cm}^{-1}$  absorption bands had similar intensities after non-catalytic oxidation and after catalytic oxidation in the presence of  $\text{Co}_3\text{O}_4$  and  $\text{Fe}_2\text{O}_3$  although the obtained carbon black conversion level in the presence of these catalysts was much higher.  $\text{CuO}$  and  $\text{V}_2\text{O}_5$  clearly caused an enhancement of the intensity of the IR bands ascribed to SOC, relative to carbon black prepared under similar conditions. Apparently, the presence of a catalyst hardly affects the band positions of the oxygen functionalities. The band intensity of the oxygen functionality formed after catalytic and non-catalytic combustion of soot cannot be compared, because there is a considerable dilution effect of soot by  $\text{V}_2\text{O}_5$ . But in all previous studies, usually KBr is used as a diluent in IR spectroscopic measurements to obtain high quality *in-situ* spectra of carbonaceous materials. It should be noted that the interactions between SOC and/or metal oxides and KBr cannot be excluded, especially when analyses are performed at elevated temperatures. While carbon black significantly absorbs IR radiation over the entire region from 400 to 4000  $\text{cm}^{-1}$ . Therefore, it is not feasible to characterize the soot combustion over metal oxides by using *in-situ* IR method.

UV Raman can be effectively applied to monitoring the reaction condition of soot combustion over transition metal oxide catalysts. Use of KBr as diluent is not necessary. *In-situ* Raman spectroscopy for the soot combustion reaction was performed at various temperatures on the  $\text{V}_4/\text{TiO}_2$  and  $\text{V}_4/\text{ZrO}_2$  catalysts, the most active catalysts among the  $\text{V}_m/\text{TiO}_2$  and  $\text{V}_m/\text{ZrO}_2$  samples of loading ratios. The Raman spectra were recorded in the range of 300—3000  $\text{cm}^{-1}$ . From 300 to 1100  $\text{cm}^{-1}$  information on the metal-oxygen vibrational modes can be obtained, while information on the soot or SOC can be gleaned from 1200 to 3000  $\text{cm}^{-1}$ . The lower wave number regions for all the supported vanadia samples did not provide any additional information and the pure oxide supports exhibited no changes in the metal-oxygen region. Raman spectra taken during the oxidation of soot clearly show that the surface oxygen species can undergo significant structural changes depending on the oxidation temperature and the composition of the sup-

port. The band centered at  $1675\text{ cm}^{-1}$  in the spectrum of  $\text{V}_4/\text{TiO}_2$  may be assigned to the  $\nu_{\text{as}}$  vibration of  $\text{NO}_2$ <sup>[36,37]</sup>. With the increase of the reaction temperature, the reaction between  $\text{NO}_2$  and soot was accelerated. As a consequence the *in-situ* UV Raman spectra of  $\text{V}_4/\text{TiO}_2$  exhibited that the intensity of the peak at  $1675\text{ cm}^{-1}$  gradually decreased from  $100^\circ\text{C}$  and the peak disappeared when the reaction temperature increased to  $300^\circ\text{C}$ . The peaks at  $1554$  and  $1608\text{ cm}^{-1}$  in the spectra of  $\text{V}_4/\text{TiO}_2$  and  $\text{V}_4/\text{ZrO}_2$  indicate the formation of SOC on Printex-U in the presence of catalyst. Unlike the reported SOC in literature where mainly quinone, lactones and ether-like complexes were identified, mainly carboxyl groups were identified as the SOC by *in-situ* UV Raman spectroscopy in this work<sup>[38–40]</sup>. Comparing Figure 5(a) and Figure 6(a) we can find that SOC on  $\text{V}_4/\text{TiO}_2$  exist at ambient temperature, while they are formed on  $\text{V}_4/\text{ZrO}_2$  until the reaction temperature reaches  $100^\circ\text{C}$ . This indicates that SOC are more easily produced on  $\text{V}_4/\text{TiO}_2$  than on  $\text{V}_4/\text{ZrO}_2$ . Similarly, the vibration peak intensities of SOC at  $1545$  and  $1618\text{ cm}^{-1}$  are much lower in Figure 7 than those in Figure 6(a). It can be concluded that SOC are more easily produced under the  $(\text{NO}+\text{O}_2)/\text{He}$  atmosphere than under the  $\text{O}_2/\text{He}$  atmosphere. The result indicates that the presence of NO in reaction gas stream can promote the production of SOC. The results of *in-situ* UV Raman demonstrate the formation of SOC is a fundamental process taking place in the catalytic soot combustion over  $\text{V}_m/\text{TiO}_2$  and  $\text{V}_m/\text{ZrO}_2$  samples.

Based on results and discussion, a reaction mechanism can be proposed:



where,  $\text{M}_x\text{O}_y$  refers to  $\text{V}_4/\text{TiO}_2$  or  $\text{V}_4/\text{ZrO}_2$  catalyst, and  $\text{C}_f$  to the surface of unreactive carbon, and  $\text{C}_f(\text{O})$  to the unreactive surface oxygen complexes, and SOC stands for the reactive surface oxygen complexes. Moreover, the difference between  $\text{O}_2$  and  $\text{O}_{\text{ads}}$  should be explicitly noticed.  $\text{O}_2$  denotes a much more free state of oxygen, being mobile on the edges or basal plane of the carbonaceous material, and  $\text{O}_{\text{ads}}$  stands for the adsorption

oxygen on the surface of catalyst. In the above notation,  $\text{C}_f(\text{O})$  and SOC refer to surface oxygen complexes in which the chemical interaction between the carbon and oxygen atom is so strong that the oxygen atom can be considered to be chemically bonded. In refs. [40–42], these surface oxygen complexes may be composed of carbonyl and ether groups in the form of lactone, quinone and acid anhydride functional groups. However, SOC are typically composed of carboxyl in this work. This mechanism is consistent with that in ref. [42].

The oxygen atoms adsorbed on soot ( $\text{O}_{\text{ads}/\text{C}}$ ) are formed by the decomposition of oxygen molecule on catalysts. They react with the soot forming of SOC. These complexes consist of carbon and oxygen atoms in different configurations, oxygen is added to such complexes through reaction, and upon desorption of a CO and/or  $\text{CO}_2$ , an adjacent carbon atom forms a new complex. Surface oxygen complexes increase the rates of catalytic oxidation of Printex-U and  $\text{CO}_2/\text{CO}$  ratios in the oxidation product also increase in the presence of surface oxygen complexes.

It is noted that the formation of SOC might explain some phenomena observed with the *in-situ* UV Raman for the catalytic combustion of soot. However, the formation of SOC is not an exclusive factor affecting on the reaction rate. In comparison of Figure 5(a) and Figure 6(a), the Raman band intensity of SOC formed on  $\text{V}_4/\text{ZrO}_2$  is stronger than that of SOC formed on  $\text{V}_4/\text{TiO}_2$ . But the reaction temperature of soot combustion over  $\text{V}_4/\text{ZrO}_2$  is higher than that of soot combustion over  $\text{V}_4/\text{TiO}_2$ . This suggests that some other factors are also influencing the soot combustion. UV-Raman result in Figure 5(a) shows the formation of  $\text{NO}_2$  in the process of soot combustion over  $\text{V}_4/\text{TiO}_2$  sample under  $(\text{NO}+\text{O}_2)/\text{He}$  atmosphere, indicating that  $\text{NO}_2$  participates in the reaction process. Some researchers demonstrated that the presence of NO in reaction gas stream can remarkably promote soot combustion over the Pt catalyst<sup>[18,19]</sup>. The NO molecule might play a role in soot combustion by the following reactions:



Due to the strong oxidation capacity of  $\text{NO}_2$ , the soot oxidation can be remarkably accelerated by  $\text{NO}_2$ . Therefore,  $\text{V}_4/\text{TiO}_2$  catalyst has higher activity than  $\text{V}_4/\text{ZrO}_2$  catalyst.

## 5 Conclusions

(1) At low V loading, the vanadium oxide species supported on TiO<sub>2</sub> or ZrO<sub>2</sub> are present in monomeric form. With the increase of V loading, polymeric vanadium species form on the surface of the samples, and when V loading reaches 4, the catalyst attains monolayer coverage on the support surface. Further increase in V loading results in the formation of V<sub>2</sub>O<sub>5</sub> crystallites. Under the condition of monolayer coverage, the catalyst exhibited the best catalytic activity.

(2) The Ultraviolet Raman spectroscopy is a powerful tool for the study of solid catalysts. The real-time formation of SOC in the heterogeneous reactions of soot oxidation with NO+O<sub>2</sub> or O<sub>2</sub> over V<sub>4</sub>/TiO<sub>2</sub> and V<sub>4</sub>/ZrO<sub>2</sub> catalysts was identified by *in-situ* UV Raman spectroscopy. The SOC species mainly existed in carboxyl groups. Moreover, the presence of NO in reaction gas stream can promote the production of SOC. On the other hand, the production of NO<sub>2</sub> in the reaction gas stream might also play an important role in the catalytic combustion of soot.

- 1 Giakoumelou I, Fountzoula C, Kordulis C, Boghosia S. Molecular structure and catalytic activity of V<sub>2</sub>O<sub>5</sub>/TiO<sub>2</sub> catalysts for the SCR of NO by NH<sub>3</sub>: *in situ* Raman spectra in the presence of O<sub>2</sub>, NH<sub>3</sub>, NO, H<sub>2</sub>, H<sub>2</sub>O, and SO<sub>2</sub>. *J Catal*, 2006, 239(1): 1–12
- 2 Wei D, Wang H, Feng X B, Chueh W, Ravikovitch P, Lyubovsky M, Li C, Takeguchi T, Haller G L. Synthesis and characterization of vanadium-substituted mesoporous molecular sieves. *J Phys Chem B*, 1999, 103(12): 2113–2121
- 3 Reddy B M, Lakshmanan P, Loridant S, Yamada Y, Kobayashi T, Lopez-Cartes C, Rojas T C, Fernandez A. Structural characterization and oxidative dehydrogenation activity of V<sub>2</sub>O<sub>5</sub>/Ce<sub>x</sub>Zr<sub>1-x</sub>O<sub>2</sub>/SiO<sub>2</sub> catalysts. *J Phys Chem B*, 2006, 110(18): 9140–9147
- 4 Zhao Z, Yamada Y, Ueda A, Sakurai H, Kobayashi T. The role of redox and acid-base properties of silica-supported vanadia catalysts in the selective oxidation of ethane. *Catal Today*, 2004, 93-95: 163–171
- 5 Xiong G, Li C. UV Raman spectroscopy and its applications in catalysis. *Chin J Light Scattering (in Chinese)*, 2000, 12: 71–76
- 6 Li C, Xiong G, Liu J, Ying P, Xin Q, Feng Z. Identifying framework titanium in TS-1 zeolite by UV resonance Raman spectroscopy. *J Phys Chem B*, 2001, 105(15): 2993–2997
- 7 Shi J, Chen J, Feng Z, Chen T, Lian Y, Wang X, Li C. Photoluminescence characteristics of TiO<sub>2</sub> and their relationship to the photoassisted reaction of water/methanol mixture. *J Phys Chem C*, 2007, 111(2): 693–699
- 8 Chen J, Feng Z, Ying P, Li C. ZnO cluster encapsulated inside micropores of zeolites studies by UV Raman and laser-induced luminescence spectroscopies. *J Phys Chem B*, 2004, 108(34): 12669–12676
- 9 Yu J, Li M, Liu Z, Feng Z, Xin Q, Li C. Comparative study of the vanadium species in VAPO-5 and VAPSO-5 molecular sieves. *J Phys Chem B*, 2002, 106(35): 8937–8943
- 10 Li C. Chiral synthesis on catalysts immobilized in microporous and mesoporous materials. *Catal Rev*, 2004, 46(3-4): 419–492
- 11 Setiabudi A, Allaart N K, Makkee M, Moulijn J A. *In situ* visible microscopic study of molten Cs<sub>2</sub>SO<sub>4</sub>-V<sub>2</sub>O<sub>5</sub>-soot system: Physical interaction, oxidation rate, and data evaluation. *Appl Catal B*, 2005, 60(3-4): 233–243
- 12 Zhao Z, Liu J, Xu C, Duan A, Kobayashi T, Wachs I E. Effects of alkali metal cations on the structures, physico-chemical properties and catalytic behaviors of silica-supported vanadium oxide catalysts for the selective oxidation of ethane and the complete oxidation of diesel soot. *Topics in Catal*, 2006, 38(4): 309–325
- 13 Liu J, Zhao Z, Xu C, Duan A, Zhu L, Wang X. Diesel soot oxidation over vanadium oxide and K-promoted vanadium oxide catalysts. *Appl Catal B*, 2005, 61(1-2): 36–46
- 14 Craenenbroeck J V, Andreeva D, Tabakova T, Werde K V, Mullens J, Verpoort F. Spectroscopic analysis of Au-V-based catalysts and their activity in the catalytic removal of diesel soot particulates. *J Catal*, 2002, 209(2): 515–527
- 15 Liu J, Zhao Z, Xu C, Duan A, Wang L, Zhang S. Synthesis of nanopowder Ce-Zr-Pr oxide solid solutions and their catalytic performances for soot combustion. *Catal Commun*, 2007, 8(3): 220–224
- 16 Yu J, Jiang Z, Zhu L, Hao Z, Xu Z. Adsorption/desorption studies of NO<sub>x</sub> on well-mixed oxides derived from Co-Mg/Al hydrotalcite-like compounds. *J Phys Chem B*, 2006, 110(9): 4291–4300
- 17 Zhu L, Wang X, Yu, J, Hao Z. Catalytic performance of K-Ce<sub>0.5</sub>Zr<sub>0.5</sub>O<sub>2</sub> catalysts for soot combustion. *Acta Phys-Chim Sin (in Chinese)*, 2005, 21(8): 840–845
- 18 Oi-Uchisawa J, Obuchi A, Wang S D, Nanba T, Ohi A. Catalytic performance of Pt/MO<sub>x</sub> loaded over SiC-DPF for soot oxidation. *Appl Catal B*, 2003, 43(2): 117–129
- 19 Oi-Uchisawa J, Obuchi A, Enomoto R, Xu J Y, Nanba T, Liu S T, Kushiyama S. Oxidation of carbon black over various Pt/MO<sub>x</sub>/SiC catalysts. *Appl Catal B*, 2001, 32(4): 257–268
- 20 Liu J, Zhao Z, Xu C, Duan A, Meng T, Bao X. Simultaneous removal of NO<sub>x</sub> and diesel Soot particulates over nanometric La<sub>2-x</sub>K<sub>x</sub>CuO<sub>4</sub> complex oxide catalysts. *Catal Today*, 2007, 119(1-4): 267–272
- 21 Dai H, He H, Li P, Gaob L, Auc C. The relationship of structural defect-redox property-catalytic performance of perovskites and their related compounds for CO and NO<sub>x</sub> removal. *Catal Today*, 2004, 90(3-4): 231–244
- 22 Shangguan W F, Teraoka Y, Kagawa S. Promotion effect of potassium on the catalytic property of CuFe<sub>2</sub>O<sub>4</sub> for the simultaneous removal of NO<sub>x</sub> and diesel soot particulate. *Appl Catal B*, 1998, 16(2): 149–154
- 23 Wang H, Zhao Z, Xu C, Liu J, Lv Z. The catalytic behavior of La-Mn-O nanoparticle perovskite-type oxide catalysts for the combustion of the soot particle from the diesel engine. *Chin Sci Bull*, 2005, 50(14): 1440–1444
- 24 Wang H, Zhao Z, Xu C, Liu J. Nanometric La<sub>1-x</sub>K<sub>x</sub>MnO<sub>3</sub> perovskite-type oxides—highly active catalysts for the combustion of diesel soot particle under loose contact conditions. *Catal Lett*, 2005, 102(3-4): 251–256

- 25 Neef J P A, Makkee M, Moulijn J A. Catalysts for the oxidation of soot from diesel exhaust gases. I. An exploratory study. *Appl Catal B*, 1996, 8(1): 57–78
- 26 Gregory T W, Ted S O, Alexis T B. Laser Raman spectroscopy of supported vanadium oxide catalysts. *J Phys Chem*, 1990, 94(10): 4240–4246
- 27 Zhang J, Li M, Feng Z, Chen J, Li C. UV Raman spectroscopic study on TiO<sub>2</sub>. I. Phase transformation at the surface and in the bulk. *J Phys Chem B*, 2006, 110(2): 927–935
- 28 Das N, Eckert H, Hu H, Wachs I E, Walzer J F, Feher F J. Bonding states of surface vanadium(V) oxide phases on silica: Structural characterization by vanadium-51 NMR and Raman spectroscopy. *J Phys Chem*, 1993, 97(31): 8240–8243
- 29 Olthof B, Khodakov A, Bell A T, Iglesia E. Effects of support composition and pretreatment conditions on the structure of vanadia dispersed on SiO<sub>2</sub>, Al<sub>2</sub>O<sub>3</sub>, TiO<sub>2</sub>, ZrO<sub>2</sub>, and HfO<sub>2</sub>. *J Phys Chem B*, 2000, 104(7): 1516–1528
- 30 Khodakov A, Yang J, Su S, Iglesia E, Bell A T. Structure and properties of vanadium oxide-zirconia catalysts for propane oxidative dehydrogenation. *J Catal*, 1998, 177(2): 343–351
- 31 Li M, Feng Z, Xiong G, Ying P, Xin Q, Li C. Phase transformation in the surface region of zirconia detected by UV Raman spectroscopy. *J Phys Chem B*, 2001, 105(34): 8107–8111
- 32 Sadezky A, Muckenhuber H, Grothe H, Niessner R, Poschl U. Raman microspectroscopy of soot and related carbonaceous materials: spectral analysis and structural information. *Carbon*, 2005, 43(8): 1731–1742
- 33 Tuinstra F, Koenig J L. Raman spectrum of graphite. *Chem Phys*, 1970, 53(3): 1126–1130
- 34 Wang Y, Alsmeyer D C, McCreery R L. Raman spectroscopy of carbon materials: Structural basis of observed spectra. *Chem Mater*, 1990, 2(5): 557–563
- 35 Alvarez-Puebla R A, Garrido J J, Aroca R F. Surface-enhanced vibrational microspectroscopy of fulvic acid micelles. *Anal Chem*, 2004, 76(23): 7118–7125
- 36 Amariei D, Coutheoux L, Rossigno S, Kappenstein C. Catalytic and thermal decomposition of ionic liquid monopropellants using a dynamic reactor: comparison of powder and sphere-shaped catalysts. *Chem Engineer Process*, 2007, 46(2): 165–174
- 37 Minogue N, Riordan E, Sodeau J R. Raman Spectroscopy as a probe of low-temperature ionic speciation in nitric and sulfuric acid stratospheric mimic systems. *J Phys Chem A*, 2003, 107(22): 4436–4444
- 38 Prinetto F, Ghiotti G, Occhiuzzi M, Indovina V. Characterization of oxidized surface phases on VO<sub>x</sub>/ZrO<sub>2</sub> catalysts. *J Phys Chem B*, 1998, 102(50): 10316–10325
- 39 Chen P, Huang F, Yun S. Optical characterization of nanocarbon phases in detonation soot and shocked graphite. *Diamond & Related Mater*, 2006, 15(9): 1400–1404
- 40 Kim U J, Furtado C A, Liu X, Chen G, Eklund P C. Raman and IR spectroscopy of chemically processed single-walled carbon nanotubes. *J Am Chem Soc*, 2005, 127(44): 15437–15445
- 41 Mul G, Kapteijn F, Moulijn J A. Catalytic oxidation of model soot by metal chlorides. *Appl Catal B*, 1997, 12(1): 33–47
- 42 Stanmore B R, Brillhac J F, Gilot P. The oxidation of soot: a review of experiments, mechanisms and models. *Carbon*, 2001, 39(15): 2247–2268